Spectrochimica Acta Part A: Molecular and Biomolecular Spectroscopy 165 (2016) 33–46

Contents lists available at ScienceDirect

Spectrochimica Acta Part A: Molecular and Biomolecular Spectroscopy

journal homepage: www.elsevier.com/locate/saa

Conformational, electronic, and spectroscopic characterization of isophthalic acid (monomer and dimer structures) experimentally and by DFT

F. Bardak [a], C. Karaca [b], S. Bilgili [a], A. Atac [a], T. Mavis [a], A.M. Asiri [c,d], M. Karabacak [e,*], E. Kose [a]

[a] Department of Physics, Celal Bayar University, Manisa, Turkey
[b] Experimental Science Applications and Research Center, Celal Bayar University, Manisa, Turkey
[c] Department of Chemistry, Faculty of Science, King Abdulaziz University, Jeddah, Saudi Arabia
[d] Center of Excellence for Advanced Materials Research, King Abdulaziz University, Jeddah, Saudi Arabia
[e] Departmant of Mechatronics Engineering, H.F.T. Technology Faculty, Celal Bayar University, Turgutlu, Manisa, Turkey

ARTICLE INFO

Article history:
Received 5 December 2014
Received in revised form 28 March 2016
Accepted 30 March 2016
Available online 5 April 2016

Keywords:
Isophthalic acid
DFT
NMR and UV–Vis spectra
Vibrational spectra
DOS and MEP

ABSTRACT

Isophthalic acid ($C_6H_4(CO_2H)_2$) is a noteworthy organic compound widely used in coating and synthesis of resins and the production of commercially important polymers such as drink plastic bottles. The effects of isophthalic acid (IPA) on human health, toxicology, and biodegradability are the main focus of many researchers. Because structural and spectroscopic investigation of molecules provides a deep understanding of interactional behaviors of compounds, this study stands for exploring those features. Therefore, the spectroscopic, structural, electronic, and thermodynamical properties of IPA were thoroughly studied in this work experimentally using UV–Vis, ^{1}H and ^{13}C NMR, FT-IR, FT-Raman and theoretically via DFT and TD-DFT calculations. The UV–Vis absorption spectrum in water was taken in the region 200–400 nm. The NMR chemical shifts (^{1}H and ^{13}C) were recorded in DMSO solution. The infrared and Raman spectra of the solid IPA were recorded in the range of 4000–400 cm^{-1} and 3500–50 cm^{-1}, respectively. DFT and TD-DFT calculations were performed at the level of B3LYP/6–311++G(d,p) in determination of geometrical structure, electronic structure analysis and normal mode. The ^{13}C and ^{1}H nuclear magnetic resonance (NMR) spectra were estimated by using the gauge-invariant atomic orbital (GIAO) method. The scaled quantum mechanics (SQM) method was used to determine the total energy distribution (TED) to assign the vibrational modes accurately. Weak interactions such as hydrogen bonding and Van der Walls were analyzed via reduced density gradient (RDG) analysis in monomeric and dimeric forms. Furthermore, the excitation energies, density of state (DOS) diagram, thermodynamical properties, molecular electro-static potential (MEP), and nonlinear optical (NLO) properties were obtained.

© 2016 Elsevier B.V. All rights reserved.

1. Introduction

Isophthalic acid/*ortho*-phthalic acid (1.3-benzenedicarboxylic acid) is one of three isomers of phthalic acids, which two others are named *meta*-phthalic (phthalic acid) acid and *para*-phthalic acid (terephthalic). It is a colorless solid organic compound that plays an important role as precursors to commercially polymers, e.g. the fire-resistant material Nomex. IPA is also used in the production of resins for drink bottles when mixed with terephthalic acid. The high performance polymer polybenzimidazole (PBI), for instance, is manufactured from isophthalic acid [1].

There are numerous studies on synthesis and production of polymers and coordination complexes based on IPA and its isomers. The following studies summarize the ongoing research on the IPA and IPA based ligands. The adsorption behavior and structure of phthalic acid and benzoic acid on the gold surface with combination of SERS and DFT calculation methods have been presented by Gao et al. [2]. Hwang et al. has investigated the adsorption of IPA at the hematite/water interface using batch adsorption experiments and ATR-FTIR spectroscopy [3]. FT-IR and Raman spectra of dimethylterephthalate as microcrystalline powder have been reported by semi empirical and ab initio calculations [4]. The molecular conformations, vibrational and electronic analysis of 2-aminoterephthalic acid derivative terephthalic acid of isophthalic acid isomer were examined using experimental technique and density functional theory calculations [5]. Many functional IPA-based and derivate coordination polymers were synthesized and structural and photoluminescence behaviors were explored because of their being good candidates for the construction of coordination polymers a series of 1D, 2D and 3D coordination polymers. [6]. Yang et al. reported that syntheses and crystal structures of two coordination polymers using hydroxylation of isophthalic acid in the hydrothermal reaction

* Corresponding author.

http://dx.doi.org/10.1016/j.saa.2016.03.050
1386-1425/© 2016 Elsevier B.V. All rights reserved.

of Cu II-isophthalate system [7]. The synthesis and characterization of poly-benzobisthiazoles derived from halogenated phthalic acid and isophthalic acid were studied by Saxena et al. [8]. The complexes of isophthalic acid also were prepared and identified by elemental analysis, IR spectroscopy and X-ray single-crystal diffraction [9]. Solubilities of terephthalaldehydic, *p*-toluic, benzoic, terephthalic, and isophthalic acids in *N*,*N*-dimethylformamide were reported as a function of temperature in the temperature range 294.75–370.45 K using a laser monitoring observation technique [10]. IPA and trimesic acid on Au (111) single crystals and on Au(111–25 nm) quasi-single crystalline film electrodes in 0.1 M $HClO_4$ were investigated via infrared reflection absorption spectroscopy (SEIRAS) and scanning tunneling microscopy (STM) with cyclic voltammetry [11]. Hamilton et al. showed that linked bis-isophthalic acid derivatives form ordered molecular structures in the solid state [12]. They also reported the design and synthesis of a novel isophthalic acid derived organogelator [13]. IPA-based mesogenic dimers were synthesized and structural effects on mesophase properties were examined [14].

The works above show that the IPA and its isomers are widely used in the synthesis of new coordination compounds and polymer systems, and the structure of the compound plays a significant role in all processes. Although there has been some works that describe the crystal structures of phthalic acid, isophthalic acid, terephthalic acid, and biphenyl-3,3,5,5-tetracarboxylic acids presented by several groups [15–17], to the best of our knowledge, there has not been any quantum chemical calculations or experimental study to report the conformational, interactional, magnetic, and electronic features of IPA. Thus, we brought wide range of spectroscopic techniques (UV–Vis, ^{1}H and ^{13}C NMR, FT-IR and Raman spectra) together to describe these characteristics of IPA with the support from DFT calculations. We used a favorite and cost-effective approach, the gradient corrected density functional theory (DFT) [18] with the Becke's three-parameter hybrid functional (B3) [19] for the exchange part and the Lee–Yang–Parr (LYP) correlation function [20], in Gaussian 09 packet program [21]. Theoretical calculations significantly enrich the accessible knowledge about the molecule such as nonlinear optical properties and thermodynamical features at very large temperature range, and help to visualize and quantify many key properties like weak interactions and potential energy surfaces. Appropriately chosen methods and basis set combinations give pretty well matching results with experimental observations as shown in this study with DFT-B3LYP/6-311G++(d,p) for calculations of geometrical and vibrational properties, TD-DFT/B3LYP/6-311G++(d,p) for electronic properties, and GIAO-B3LYP/6-311G++(d,p) for magnetic features, all generating appreciable results.

The rest of the paper is organized as follows; experimental details are presented in Experimental details section. The computational method is given in Computational details section. The experimental and simulation results for monomer and dimer structural, electronic properties, chemical shifts and vibrational features, thermodynamic properties for the title molecule considered in this study are presented and discussed in the section of Results and discussion. We have also compared the simulation results with the observed data in the same Section. Finally, the summary of our main results are given in the last section.

2. Experimental details

IPA molecule is supplied from Across Organics Company in solid state with a purity of 99% and used without any further purification. UV–Vis (200–400 nm) spectrum in water was recorded by using Shimadzu UV-2101 PC, UV—VIS recording Spectrometer. NMR (^{1}H and ^{13}C) spectra were obtained in Varian Infinity Plus spectrometer at 300 K, in DMSO. The NMR chemical shifts are reported in ppm relative to tetramethylsilane (TMS). FT-IR (4000–400 cm^{-1}) spectrum is recorded in Perkin-Elmer FT-IR System Spectrum BX spectrometer by using a KBr disc technique with a scanning speed of 10 cm^{-1} min^{-1} and the spectral resolution of 4.0 cm^{-1}. FT-Raman (3500–10 cm^{-1}) spectrum of the title molecule is recorded in Bruker RFS 100/S FT-Raman instrument using 1064 nm excitation from an Nd:YAG laser with a liquid nitrogen cooled Ge detector by accumulating five hundred scans at 4 cm^{-1} resolution at a laser power of 100 mW.

3. Computational details

All calculations presented in this study were performed by using Gaussian 09 software [21]. A total of 10 different conformations of monomeric IPA for C_1, and 7 that of Cs, and 4 conformations for C_{2v} symmetry group were optimized and frequencies were computed by using DFT/B3LYP level of theory with 6-311++G(d,p) basis set. The structure and frequencies of dimeric structure for the most stable conformation of IPA were also determined. The calculated wavenumbers in the ranges from 4000 to 1700 cm^{-1} and that of lower than 1700 cm^{-1} are scaled with 0.958 and 0.983, respectively [22,23]. The UV–Vis spectra, electronic transitions, vertical excitation energies, absorbance, and oscillator strengths with help of Time Dependent-DFT [24–26] for gas phase and in water solvent environment of the Polarizable Continuum Model (PCM) using the integral equation formalism variant (IEFPCM). ^{1}H and ^{13}C NMR chemical shifts were calculated using the GIAO method [27,28] in DMSO for both monomeric and dimeric structures. Relative chemical shifts are estimated by using corresponding TMS shielding calculated in advance at the same theoretical level as the reference. The total energy distributions were calculated by using the scaled quantum mechanics scaled quantum mechanics method and PQS program [29,30] in order to characterize of fundamental vibrational modes.

GaussSum 2.2 [31] was utilized to plot density of states; the total (TDOS), the partial density of states (PDOS), and overlap population density of states (OPDOS or COOP) diagrams, and to have analysis group contributions of molecular orbitals using Mulliken population analysis. The PDOS and OPDOS graphs were obtained by convoluting the molecular orbital information with Gaussian curves of unit height and a FWHM (Full Width at Half Maximum) of 0.3 eV. Electrostatic potential map is calculated with use of QMFORGE and Multiwfn programs [32,33]. The Reduced density gradient of the title molecule (monomer and dimer forms) are graphed by Multiwfn [32] and plotted by VMD program [34]. Besides, the statistical thermodynamic functions (the heat capacity, entropy, and enthalpy) and nonlinear optical (NLO) properties of IPA are obtained from the frequency calculations by repeating at different temperatures and including the polarizability derivative calculations, respectively.

4. Results and discussion

4.1. Energy conformers

Ten possible conformers of IPA molecule depending on the position and orientation of hydroxyl fragment in carboxyl group are illustrated in Fig. 1(a–c). All optimizations are carried out for C_{2v}, C_s and C_1 symmetries as input orientation leads to a linear conformation but C_{2v} and C_s conformers have transition states with one or two imaginary wavenumbers. To determine which conformer is at minimum among all, we use the formula $\Delta E = E(Cnm) - E(C11)$ and listed the values in Table 1. The regarding table shows that some conformers have quite small differences in energy. All conformers' energies are also highly close in energy in terms of the both symmetry and orientations. The lowest energy is obtained for the C11 conformer in C_s point group with −609.58387910 Hartree (−382519.6752 kcal/mol). The next closest energy is achieved with C11 conformer in C_{2v} symmetry with −609.58387800 Hartree (−382519.6745 kcal/mol). The difference between the energies of these two geometries is only 0.0007 kcal/mol. This can even be ignored because it is nearly at least thousand times less than the energy difference between different conformers. The lowest energy judgement is not always to be an appropriate decision maker

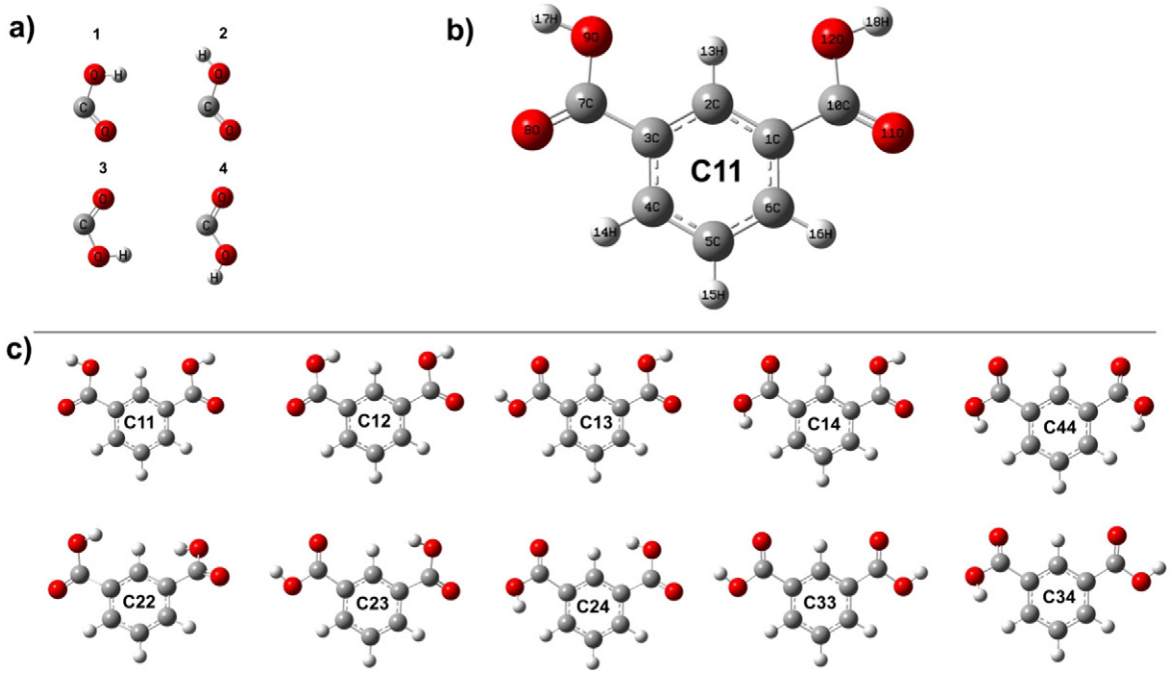

Fig. 1. a) The possible orientations of carboxyl group, b) The most stable structure of IPA in C_{2v} point group, c) The optimized structures of IPA for ten possible conformations.

to select which symmetry should be chosen. Therefore, we consider the entropy of these geometries. The total entropy of C11 geometry in C_{2v} symmetry is 98.917 cal·mol^{-1} K^{-1} whereas that of in Cs is 100.289 cal·mol^{-1} K^{-1}. It is well known that the universe evolves towards a maximum symmetry as stated in Shu-Kun Lin's work on correlation of entropy and symmetry [35] and the highest symmetry results in lower entropy due to loss of information about the system by the reduction of positional degeneracy. Furthermore, this geometry also has nearly zero dipole moment which is significantly different than that of the other geometries. However, there is no consensus on a direct correlation between the molecular dipole moment and the structural stability. Here, the C11 geometry with C_{2v} symmetry given in Fig 1(b), therefore, should be chosen as the most abundant and possible geometry for IPA molecule. Thus, all calculations such as vibrational spectra, NMR, UV–Vis, and some electronic properties were based on this conformer.

4.2. Geometrical structures

The optimized monomer and dimer molecular structures of IPA along with the numbering scheme of the atoms are shown in Figs. 1(b) & 2. The calculated geometrical parameters for monomeric structure of IPA are listed in Table 2 in comparison with crystal data obtained by Derissen [16]. The bond lengths and angles obtained by

Table 1
The energies (possible conformers) and energy differences based on the most stable conformers with C_{2v}, C_s, and C_1 symmetries of IPA by DFT (B3LYP/6-311++G(d,p)) method.

Conformers		Energy		Energy differences[a]		Dipole moment
C_{2v} symmetry	Imaginary Freq. (cm^{-1})	(Hartree)	(kcal/mol)	(Hartree)	(kcal/mol)	(Debye)
C11	0	−609.58387800	−382519.6745	0.0000	0.0000	0.0002
C33	0	−609.58307501	−382519.1706	0.0008	0.5039	3.7590
C22	(−147, −187)	−609.55741331	−382503.0676	0.0265	16.6068	0.1090
C44	(−104, −116)	−609.55748617	−382503.1134	0.0264	16.5611	8.3800
C_s symmetry						
C11	0	−609.58387910	−382519.6752	0.0000	0.0000	0.9429
C13	0	−609.58363168	−382519.5199	0.0002	0.1553	1.9472
C33	0	−609.58307892	−382519.1731	0.0008	0.5021	3.7587
C23	(−77)	−609.57297641	−382512.8336	0.0109	6.8415	4.8812
C12	(−87)	−609.57243447	−382512.4936	0.0114	7.1816	3.1321
C14	(−101)	−609.57137771	−382511.8304	0.0125	7.8447	3.7503
C44	(−99, −116)	−609.55740815	−382503.0644	0.0265	16.6108	8.3849
C_1 symmetry						
C11	0	−609.58381233	−382519.6333	0.0000	0.0000	0.9383
C13	0	−609.58362610	−382519.5164	0.0002	0.1169	1.9487
C33	0	−609.58307914	−382519.1732	0.0007	0.4601	3.7569
C23	0	−609.57321830	−382512.9854	0.0106	6.6479	4.9121
C12	0	−609.57285152	−382512.7553	0.0110	6.8780	3.1132
C14	0	−609.57197366	−382512.2044	0.0118	7.4289	3.6510
C34	0	−609.57124700	−382511.7484	0.0126	7.8849	6.2254
C24	0	−609.56150454	−382505.6349	0.0223	13.9984	4.7225
C22	0	−609.56007521	−382504.7380	0.0237	14.8953	0.8054
C44	0	−609.55919163	−382504.1836	0.0246	15.4479	7.5787

[a] Energies of the other conformers relative to the most stable structure of C11 conformer.

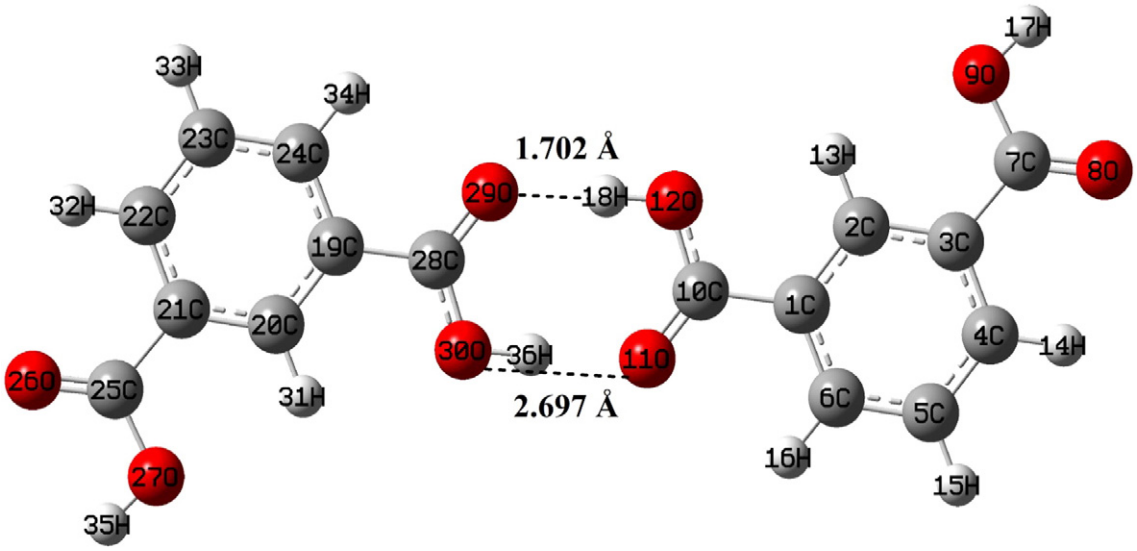

Fig. 2. Theoretical dimer structure of C11 conformer of IPA.

B3LYP/6-311++G(d,p) basis set correlate greatly with experimental values. Deviation in bond lengths is highest for CH bonds on the ring ($\Delta d_{average} \cong 0.15$ Å) while the bond angles deviates in carboxyl groups at most ($\Delta\delta_{average} \cong 3.05°$). These deviations are in the nature of theoretical calculations because the molecular geometry is calculated for the gas phase which does not take extends of hydrogen bindings and stacking interactions into account. The deviation in bond angles is actually only $\Delta\delta_{average} \cong 1.2°$ when compared with the results of dimeric structure where the intermolecular interactions treaded better.

As can be seen from Table 2, the calculated bond angle values are in harmony with the experimental bond angles. In particularly, C—C—C bond angles belonging to the ring are in very good agreement with crystal data of the compound. For example, C_1—C_6—C_5 angle value was calculated as 120.1° and observed as 120.1°. C_2—C_3—C_4, C_4—C_5—C_6 bond angles are theoretically 120.0° and experimentally 119.7°, 120.7° respectively. However, towards the carboxylic group, harmony between theoretical and experimental bond angle values is gradually decreased. Some of bond distances of benzene ring are theoretically 1.399 Å (C_1—C_6), 1.397 Å (C_2—C_3), 1.489 Å (C_1—C_{10}, C_3—C_7) and 1.390 Å (C_1—C_6), 1.386 Å (C_2—C_3), 1.475 Å (C_1—C_{10}) and 1.485 Å (C_3—C_7) in experiment, respectively. Besides, the coherence between theoretical and experimental values decreases towards the carboxylic group for bond lengths as well as bond angles. For instance, C_7—C_9 and C_{10}—O_{12} bond lengths are theoretically 1.356 Å, and experimentally 1.290 Å, and 1.298 Å.

Several authors [36,37] have explained the changes in wavenumber or bond length of the C—H bond on substitution due to a change in the charge distribution on the carbon atom of the benzene ring. The carbon

Table 2
The experimental and optimized bond lengths (Å) and angles (°) of IPA for monomer and dimer structures by using B3LYP/6-311++G(d,p).

Bond lengths (Å)	X-ray[a]	Monomer	Dimer	Bond angles (°)	X-ray[a]	Monomer	Dimer
C_1—C_2	1.379	1.397	1.397	C_3—C_4—C_5	119.6	120.1	120.2
C_1—C_6	1.390	1.399	1.400	C_3—C_4—H_{14}	118.5	118.8	118.8
C_1—C_{10}	1.475	1.489	1.487	C_4—C_5—C_6	120.7	120.0	120.0
C_2—C_3	1.386	1.397	1.397	C_4—C_5—H_{15}	121.0	120.0	120.0
C_2—H_{13}	0.900	1.08	1.081	C_1—C_6—C_5	120.1	120.1	120.1
C_3—C_4	–	1.399	1.400	C_1—C_6—H_{16}	115.8	118.8	118.9
C_3—C_7	1.485	1.489	1.488	C_3—C_7—O_9	116.1	113.0	112.9
C_4—C_5	1.375	1.391	1.391	C_7—O_9—H_{17}	110.0	106.9	107.4
C_4—H_{14}	0.920	1.083	1.084	C_1—C_{10}—O_{11}	122.0	124.8	122.3
C_5—C_6	1.371	1.391	1.391	C_{10}—O_{12}—H_{18}	110.1	106.9	110.6
C_5—H_{15}	0.930	1.084	1.085	C_2—C_1—C_{10}	–	121.3	121.3
C_6—H_{16}	0.940	1.083	1.084	C_2—C_3—C_7	–	121.9	122.0
C_7—O_8	1.231	1.208	1.209	C_1—C_2—H_{13}	–	120.1	119.9
C_7—O_9	1.290	1.356	1.355	C_1—C_{10}—O_{12}	–	113.0	114.3
O_9—H_{17}	0.980	0.969	0.970	C_{11}—C_{10}—O_{12}	–	122.2	123.5
C_{10}—O_{11}	1.234	1.208	1.228	C_5—C_4—H_{14}	–	121.1	121.0
C_{10}—O_{12}	1.298	1.356	1.323	C_5—C_6—H_{16}	–	121.1	121.0
O_{12}—H_{18}	0.970	0.969	0.995	C_6—C_5—H_{15}	–	120.0	120.0
				C_3—C_7—O_8	–	122.2	124.9

Bond angles (°)	X-ray[a]	Monomer	Dimer	Intermolecular H bonds	Bond lengths	Bond angles
C_2—C_1—C_6	119.5	120.0	120.0	O_{12}—H_{18}···O_{29}	1.703	0
C_6—C_1—C_{10}	121.3	118.0	118.7	O_{30}—H_{36}···O_{11}	2.698	180.0
C_1—C_2—C_3	120.4	119.7	119.8			
C_3—C_2—H_{13}	118.9	120.1	120.3			
C_2—C_3—C_4	119.7	120.0	119.9			
C_4—C_3—C_7	121.8	118.0	118.0			

[a] The X-ray data from Ref. [16].

atoms are bonded to the hydrogen atoms with a σ bond in benzene, and the substitution of a halogen for hydrogen reduces the electron density at the ring carbon atom. The ring carbon atoms in substituted benzenes exert a larger attraction on the valence electron cloud of the hydrogen atom resulting in an increase in the C—H force constant and a decrease in the corresponding bond length. The perceivable ones are for the bond distances of C—H among which the largest difference is 0.108 Å.

The O—H bonds for the title molecule are about equal to the experimental values. These bond lengths were calculated at 0.969 Å for O_{12}—H_{18} and O_9—H_{17}. Experimental values are observed O—H bonds are 0.970 Å and 0.980 Å. But, no experimental geometric dimer structure of IPA is published in the literature yet. Therefore, we could not compare the calculation results for dimer structure with the experimental data. The intra-molecular hydrogen bonds between the hydroxyl groups and the oxygen atoms of the carbonyl groups are strongly bent (the O—H···O angle equals 180.0°) and the O···O distance is 2.698 Å. Hydrogen bond with the intermolecular is 1.702 Å.

The linearity between the experimental and calculated bond lengths and angles of monomer and dimer structures of IPA can be estimated from plotting the calculated values against experimental ones as given in Fig. S1. The calculations provide good linearity with experimental values. The relations between theoretical and experimental values of the title molecule for monomer and dimer structures are described by the following equations, respectively.

$$d_{cal.} = 0.7578 d_{exp.} + 0.34363 \left(R^2 = 0.9218\right) \text{ for monomer structure}$$

$$d_{cal.} = 1.235 d_{exp.} - 0.3487 \left(R^2 = 0.9284\right) \text{ for dimer structure}$$

$$\delta_{cal.} = 1.772 \delta_{exp.} - 21.626 \left(R^2 = 0.8207\right) \text{ for monomer structure}$$

$$\delta_{cal.} = 0.9457 \delta_{exp.} + 6.0294 \left(R^2 = 0.7360\right) \text{ for dimer structure}$$

4.3. Electronic properties

4.3.1. RDG

Johnson et al. [38] developed an approach to investigate the weak interactions in real space based on the electron density and its derivatives. The RDG is a fundamental dimensionless quantity coming from the density and its first derivative:

$$RDG(r) = \frac{1}{2\left(3\pi^2\right)^{1/3}} \frac{|\nabla\rho(r)|}{\rho(r)^{4/3}}.$$

The weak interactions can be isolated as regions with low electron density and low RDG value. The density values of the low-gradient spikes (the plot of RDG versus ρ) appear to be an indicator of the interaction strength. The sign of λ_2 is utilized to distinguish the bonded ($\lambda_2 < 0$) from nonbonding ($\lambda_2 > 0$) interactions. The plot of the RDG versus the electron density ρ multiplied by the sign of λ_2 can allow analysis and visualization of a wide range of interactions types. The results were calculated by Multiwfn and plotted by VMD program [39] and [34], respectively.

One or more spikes are found in the low-density, low gradient region as seen in Fig. 3, indicative of weak interactions in the system and the electron density value at the RDG versus sign $(\lambda_2)\rho$ peaks itself provides the information about the strength of interaction. Large, negative values of sign $(\lambda_2)\rho$ are indicative of stronger attractive interactions and also we can identify different type of regions by color as can be seen from Fig. 4. The bluer means the stronger interactive interaction, the partial half elliptical slab between oxygen and hydrogen shows blue color, but there were no strong hydrogen in the IPA. The interaction

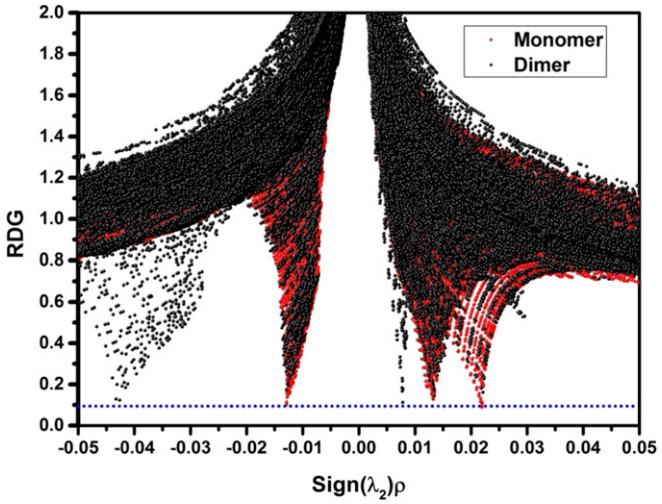

Fig. 3. Plots of the RDG versus the electron density ρ multiplied by the sign of λ_2 for both monomeric and dimeric structures of IPA. (For interpretation of the references to color in this figure, the reader is referred to the web version of this article).

region marked by green can be identified as Van der Walls (VDW) interaction region and the regions in the center of rings and the others show strong steric effect. The RDG = 0.1 lines cross not only the attractive but also the repulsion spikes. The more blue means the stronger interactive interaction, the partial half elliptical slab between oxygen and hydrogen shows blue color, so the low-density, low-reduced gradient trough in the hydrogen bonded IPA dimer lies at negative values, indicative of an attractive interaction seen in Fig. 3 and there were strong hydrogen bond between O_{12}···H_{18} and O_{11}···H_{36}, characterized by very low and almost constant electron density values, appear in regions in between the interacting molecules.

4.3.2. Molecular orbital density of states and energy

The most important application of the DOS plots is to demonstrate molecule orbital (MO) compositions and their contributions to chemical bonding through the OPDOS plots, which are also referred in the literature as COOP diagrams. The COOP (or OPDOS) is similar to DOS because it results from multiplying DOS by the overlap population. The OPDOS shows the bonding, anti-bonding and nonbonding interaction of the two orbitals, atoms or groups. A positive value of the COOP indicates a bonding interaction, whereas negative value means an anti-bonding interaction and zero value indicates nonbonding interactions [40]. The partial density of state plot mainly presents the composition of the fragment orbitals contributing to the molecular orbitals as seen from Fig. 5. Both the highest occupied molecular orbital (HOMO) and lowest unoccupied molecular orbital (LUMO) are the main orbital taking part in chemical reaction. The result provides a pictorial representation of MO compositions and their contributions to chemical bonding. The OPDOS diagram is shown in Fig. 6 and in the frontier occupied and virtual molecular orbitals, values of the interaction between ring and COOH is selected. The benzene ring shows weakest anti-bonding properties COOH groups in the IPA. As can be seen from OPDOS plot in the LUMO molecular orbitals have bonding character. The interaction of the ring with COOH orbitals has almost all a non-bonding character according to the given energy regions. The overlap population value of the HOMO for ring with COOH is −0.0254 according to this diagram. As can be seen from OPDOS LUMO overlap population value is 0.03339.

The DOS and PDOS in terms of Mulliken population analysis was calculated using Gausssum program [31]. The results provide a pictorial representation of MOs. The PDOS diagram may enable us to ascertain the orbital composition characteristics with respect to the particular fragments. The ring atoms play significant role in the HOMOs. For instance, the orbitals of the iodine atom contribute at 86% in the HOMO

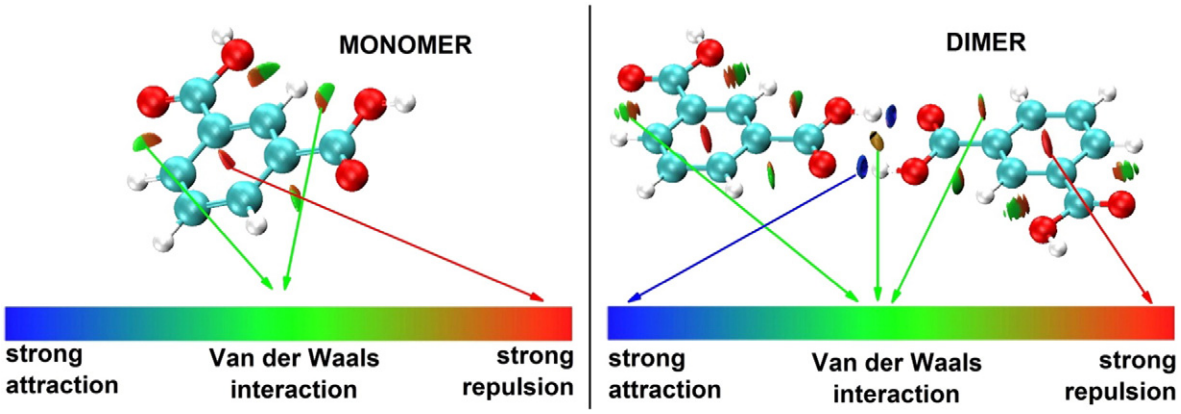

Fig. 4. Color scaling of weak interactions. The surfaces are colored on a blue–green–red scale according to values of sign λ_2. Blue indicates strong attractive interactions and red indicates strong non-bonded overlap. (For interpretation of the references to color in this figure legend, the reader is referred to the web version of this article).

(A_2 *sym.*), at 97% (B_1 *sym.*) in the HOMO − 1, at 14% in the HOMO − 2 (B_2 *sym.*) and at 13% in the HOMO − 3 (A_1 *sym.*) molecular orbitals of IPA. According to the Mulliken population analysis the COOH groups play dominant role (63%) if compared with the other groups in the LUMO (A_2 *sym.*).

4.3.3. UV–Vis spectra

The theoretical absorption spectrum obtained from the calculation of the singlet excited states by using TD-DFT calculations with the B3LYP/6-311++G(d,p) method and through experiment is shown in Fig. 7. Theoretical calculations were performed for gas phase and in water solvent environment in IEFPCM model whereas the experimental spectrum is recorded only in water solution. Theoretical treatment of electronic transitions indicates that there should be four major transitions in the region where the experimental spectrum is recorded. The most possible transitions are listed in Table 3 in comparison with the corresponding experimental values. Quantification of the experimental UV–Vis spectrum was performed using a multicomponent analysis method, which has been used successfully in describing peak result from multiple interactions [41,42]. Intensity, I, of the spectrum is modeled as a superposition of antisymmetrized Gaussian (AG) line shape functions, thus matches the peaks to major transition more accurately.

$$I_{AG}(\omega) = A_{AG}\left\{\exp\left[-(\omega-\omega_{AG})^2/2\varepsilon^2\right] - \exp\left[-(\omega+\omega_{AG})^2/2\varepsilon^2\right]\right\}.$$

This fitting procedure is applied to the theoretical data first. Comparison of the wavelength values obtained through calculations and fitting procedure in Table 3 shows clearly that the procedure followed here is nearly perfect. Then the experimental spectrum is fitted with the same number of bands. Although the experimental and calculated spectra are similar in shape, the peak positions differ significantly. The TD-DFT method predicted the maximum absorption peak at 262.91 nm while this peak was recorded at 275.94 nm experimentally in water solution, i.e. ~13 nm red shifted. Another stronger peak was calculated at 236.16 nm, which is obtained to exist at 227.57 nm, i.e. ~7 nm blue shifted. The other two transitions occur at very near region, thus appears as a single peak in total spectra; 218.1 nm and 205.6 nm in calculated and observed spectra, respectively. This peak is the best predicted peak among all with only ~3 nm deviation. Basically, the stronger peak intensity means the better prediction. All transitions occur simply between nearest frontier orbitals from HOMO − 1 to LUMO + 1. Determining factor of transition energies is the contributions of transitions rather than the type. For example, the transitions with the lowest energy and the highest energy are both results from the combination of HOMO → LUMO, HOMO − 1 → LUMO + 1 excitations; however the contributions are nearly inverse. In the case of dimer structure, peaks results from transitions between first frontier orbitals as well as the further orbitals. For example, transitions from HOMO − 2 to LUMO levels play a significant role in the existence of all peaks. In view of the calculated absorption spectra, the maximum absorption wavelength corresponds to the electronic transition from the H → L %73 and

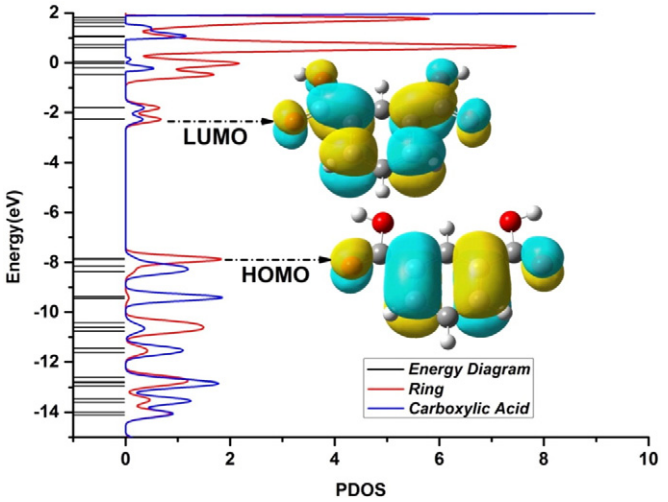

Fig. 5. The partial electronic density of states diagram of IPA.

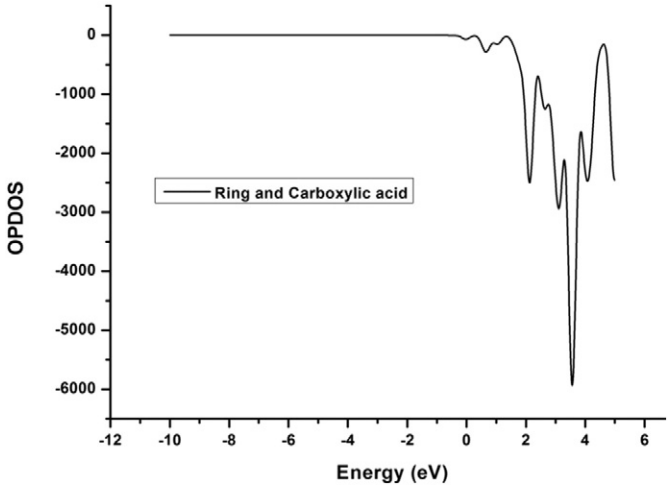

Fig. 6. Overlap population density of states curve between ring and carboxylic acid groups.

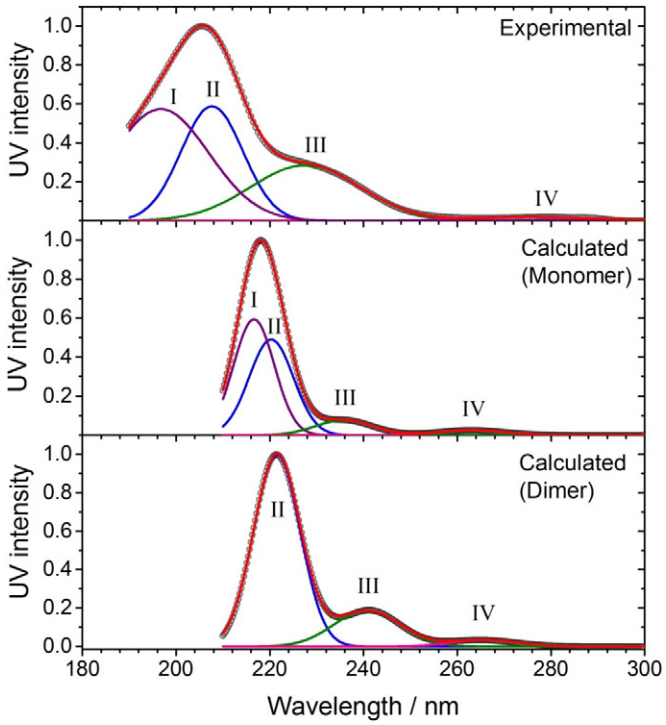

Fig. 7. Experimental and calculated UV spectra of IPA as resolved into individual electronic transitions via antisymmetrized Gaussians fitting methodology.

H − 1 → L + 1%25 contribute. The other electronic transition and their energy gaps were shown in Fig. 8 and corresponding energy and band gap values were listed in Table 4.

The energy gap between the highest occupied and the lowest unoccupied molecular orbitals is a critical parameter in determining molecular electrical transport properties because it is a measure of electron conductivity [43]. The energy gap for HOMO–LUMO is calculated as 5.63 eV. The other important energy gaps of FMOs of IPA molecule are gathered in Table 4. The charge density of HOMO localized all ring and only one oxygen atom, but the LUMO is characterized by a charge distribution all of the surfaces of molecule. Moreover, the values of chemical hardness, electronegativity, chemical potential and electrophilicity index are compared in gas phase, and water solutions are gathered in Table 4.

4.3.4. Molecular electrostatic potential

In the present study, 3D plots of molecular electrostatic potential (MEP or ESP) of IPA is illustrated in Fig. 9. The MEP is a useful property to study reactivity given that an approaching electrophile will be attracted to negative regions (where the electron distribution effect is dominant). The importance of MEP lies in the fact that it simultaneously displays molecular size, shape as well as positive, negative and neutral electrostatic potential regions in terms of color grading, and is very useful in research of molecular structure with its physiochemical property relationship. Some critical points (red and blue spheres correspond to maxima and minima respectively) within this surface are shown in Fig. 10 and its values are presented in Table 5 by computing Monte Carlo method. The blue point 5 which is the global minimum on the surface has value of −30.3102 kcal/mol whereas the red point 7 is (51.78808 kcal/mol) the global maximum arise from the abundant π electrons around the ring.

4.4. NMR spectra

NMR spectroscopy is a research technique that exploits the magnetic properties of certain atomic nuclei. It relies on the phenomenon of nuclear magnetic resonance and can provide detailed information about the structure, dynamics, reaction state, and chemical environment of molecules. The optimized structure of the studied molecule is used to calculate the NMR spectra at the DFT/B3LYP method and 6-311++G(d,p) basis set. The recorded ^{1}H and ^{13}C NMR spectra of IPA in DMSO solution are shown in Fig S2. The experimental and theoretical chemical shifts (^{1}H and ^{13}C NMR) of the present molecule (both monomer and dimer forms) in are summarized in Table 6. The isotropic shielding values are used to calculate the isotropic chemical shifts with respect to tetramethylsilane (TMS), ($\delta_{iso} = \sigma_{iso}^{TMS} - \sigma_{iso}^{x}$).

As seen from Fig. 1, the studied compound has eight carbon atoms, however, only five signals observed in the ^{13}C NMR spectrum and in calculation for the monomer in spite six carbon signals calculated for the dimer structure. Basically, C4 and C6, and C7 and C10 are the same type, thus, produce a single peak. However, C7 and C10 produce significantly different peaks in dimer structure because the environment of the nuclei changes greatly.

Similarly, although the molecule has six hydrogen atoms, four proton signals are observed in the ^{1}H NMR spectrum. This case stem from the symmetry of two carboxylic groups.

Aromatic carbons give signals in overlapped areas of the spectrum with chemical shift values from 100 to 150 ppm [44,45]. In this work, the experimental chemical shift values of aromatic ring carbons are in the range of 129.58–133.96 ppm and these values are in harmony with theoretical results. For example, C_1, C_3 and C_4, C_6 shift values were observed at 133.96, 131.84 ppm and calculated at 134.82 and 138.94 ppm respectively. On the other side, oxygen atom shows electronegative property. Therefore, the chemical shift value of C7 and C10 was observed at 167.25 ppm (C = O) and calculated (with respect to TMS) 177.59 ppm, 171.27 and 177.41 ppm for monomer and dimer structures of IPA by using B3LYP method (in Table 6). The calculated monomer and dimer ^{13}C NMR chemical shifts of the present molecule were showed the same parallel.

The chemical shifts of aromatic protons of organic molecules are usually observed in the range of 7.00–8.00 ppm [44,46]. The studied molecule has four hydrogen atoms in the ring and two hydrogen

Table 3
Experimental and calculated wavelengths λ (nm), excitation energies (eV), oscillator strengths (*f*) of IPA, in water.

TD-DFT/B3LYP/6-311++G(d,p) (water)						Experimental (water)	
Band	λ (nm) fitted	λ (nm) calculated	E (eV)	*f*	Major contributes	λ (nm) fitted	E (eV)
Monomer							
I	216.61	217.90	5.6900	0.8615	H − 1 → L + 1 (71%), H → L (22%)	196.72	6.3026
II	220.29	219.31	5.6534	0.1465	H → L + 1 (68%), H − 1 → L (25%)	207.66	5.9705
III	235.82	236.16	5.2500	0.0763	H − 1 → L (72%), H → L + 1 (27%)	227.57	5.4482
IV	263.09	262.91	4.7158	0.0263	H → L (73%), H − 1 → L + 1 (25%)	275.94	4.4932
Dimer							
II	221.50	221.41	5.59976	1.4689	H − 2 → L + 2 (53%), H − 1 → L + 1 (13%)		
III	240.78	242.09	5.12141	0.2432	H − 2 → L (65%), H → L (13%)		
IV	265.90	265.08	4.67724	0.0502	H → L (40%), H − 1 → L + 1 (30%), H − 2 → L + 2 (13%)		

H: HOMO, L: LUMO.

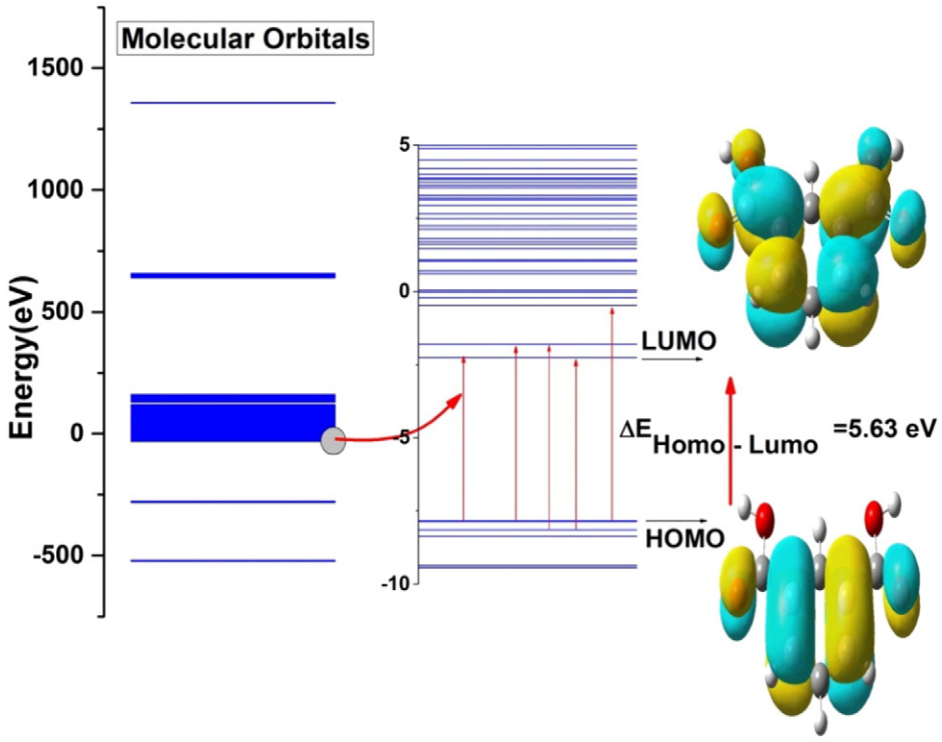

Fig. 8. All molecular orbital energies of IPA with some electronic transitions.

atoms attached to the oxygen atom of carboxylic group. As can be seen from Table 6, ^{1}H chemical shifts were observed at 8.46 (H13), 8.11 (H14 and H16), 7.55 (H15) ppm and calculated at 9.16, 8.23 and 7.75 ppm respectively for aromatic ring. The proton chemical shifts in the ring are calculated in the range of 8.57–9.96 ppm for dimer structure. The chemical shift of OH is very dependent on solvent and other experimental conditions. Resulting of the integration of the signal around 13 ppm as two while that of near 8 ppm gives one indicates that the proton, resonances at 13 ppm (H18), corresponds to two acidic protons of IPA.

The correlation graphics between the experimental and calculated chemical shifts for monomer and dimer structures of the title molecule are represented in Fig. S3. The relations between the calculated (monomer and dimer) and experimental chemical shifts (δ_{exp}) are usually linear and described by the following equation:

$$\delta_{cal}(ppm) = 0.9553\delta_{exp} + 0.5732 \left(R^2 = 0.9986\right) \text{ Monomer}$$

$$\delta_{cal}(ppm) = 0.9689\delta_{exp} - 0.6220 \left(R^2 = 0.9978\right) \text{ Dimer.}$$

In the present study, the following linear relationships were obtained for monomer and dimer structures for ^{1}H and ^{13}C chemical shifts.

For monomer structure

$$\delta_{cal}(ppm) = 0.5915\delta_{exp} + 3.1229 \,^{1}\text{H NMR;} \left(R^2 = 0.8599\right)$$

Table 4
The calculated energies values of IPA molecule using by the TD-DFT/B3LYP method using 6-311++G(d,p) basis set.

	Monomer		Dimer	
TD-DFT/B3LYP/6–311++G(d,p)	Gas	Water	Gas	Water
E_{total} (Hartree)	−609.5733	−609.5863	−1219.1560	−1219.1730
E_{HOMO-2} (eV)	−8.09	−8.23	−7.86	−7.83
E_{HOMO-1} (eV)	−8.02	−7.96	−7.86	−7.80
E_{HOMO} (eV)	−7.95	−7.84	−7.86	−7.79
E_{LUMO} (eV)	−2.32	−2.28	−2.32	−2.30
E_{LUMO+1} (eV)	−1.90	−1.88	−2.25	−2.23
E_{LUMO+2} (eV)	−0.47	−0.31	−1.84	−1.84
$E_{HOMO-LUMO\ gap}$ (eV)	5.63	5.56	5.54	5.49
$E_{HOMO-LUMO+1\ gap}$ (eV)	6.05	5.96	5.61	5.56
$E_{HOMO-LUMO+2\ gap}$ (eV)	7.48	7.53	6.02	5.95
$E_{HOMO-1-LUMO\ gap}$ (eV)	5.70	5.68	5.54	5.50
$E_{HOMOs1-LUMO+1\ gap}$ (eV)	6.12	6.08	5.61	5.57
$E_{HOMOs1-LUMO+2\ gap}$ (eV)	7.55	7.65	6.02	5.96
$E_{HOMOs2-LUMO\ gap}$ (eV)	5.77	5.95	5.54	5.53
$E_{HOMOs2-LUMO+2\ gap}$ (eV)	7.62	7.92	6.02	5.99
Chemical hardness (h)	2.82	2.78	2.77	2.75
Electronegativity (χ)	5.14	5.06	5.09	5.05
Chemical potential (μ)	−5.14	−5.06	−5.09	−5.05
Electrophilicity index (ω)	4.68	4.60	4.68	4.64

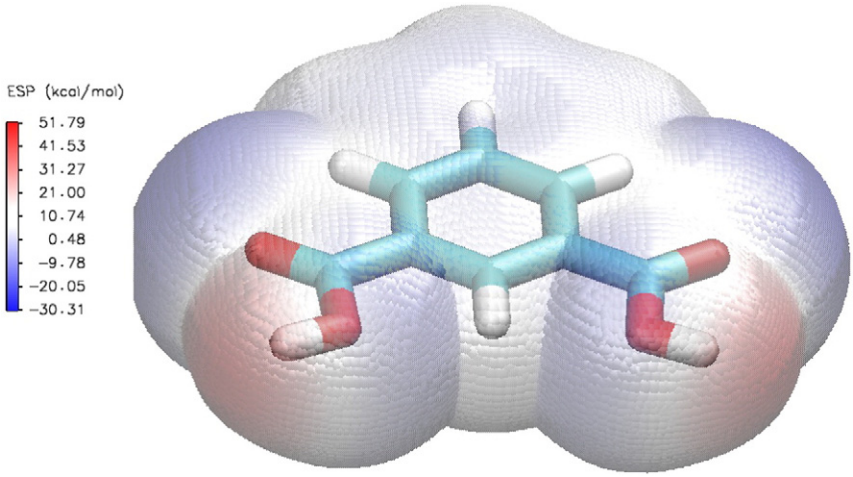

Fig. 9. MEP or ESP-mapped molecular VDW surface of IPA.

$$\delta_{cal}(ppm) = 0.8464\delta_{exp} + 16.668\ ^{13}C\ NMR;\ \left(R^2 = 0.9784\right)$$

For dimer structure

$$\delta_{cal}(ppm) = 1.0803\delta_{exp} - 2.0377\ ^{1}H\ NMR;\ \left(R^2 = 0.9894\right)$$

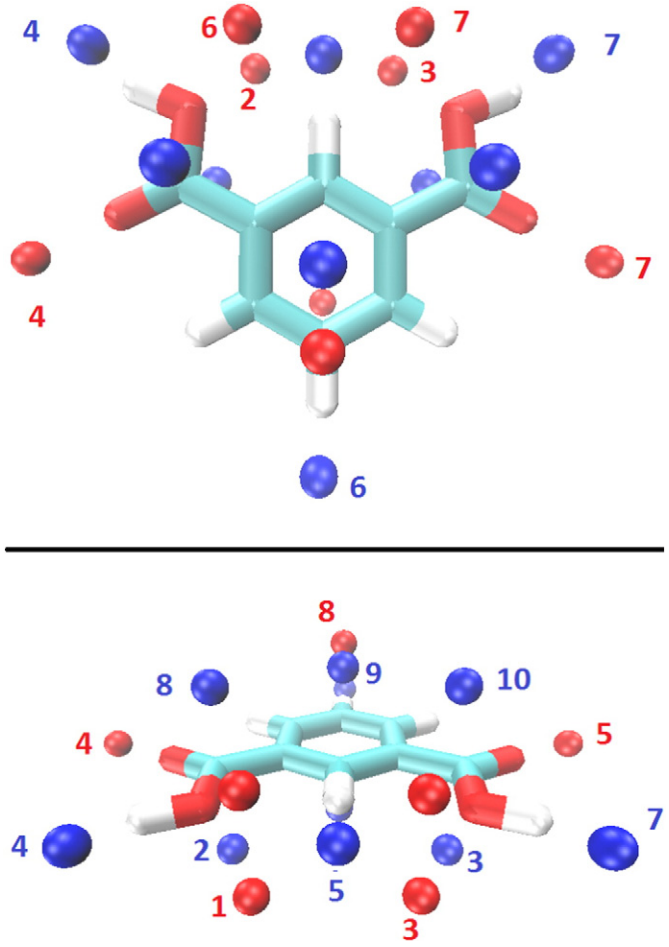

Fig. 10. Surfaces local minima and maxima of MEP or ESP of IPA are represented red and blue spheres, respectively. (For interpretation of the references to color in this figure, the reader is referred to the web version of this article.)

$$\delta_{cal}(ppm) = 0.8827\delta_{exp} + 12.244\ ^{13}C\ NMR;\ \left(R^2 = 0.9432\right).$$

The performances of the B3LYP method with respect to the prediction of the chemical shifts within the molecule are quite close.

4.5. Vibrational spectral analysis

The IPA has 18 atoms and C_{2v} symmetry group. Its fundamental vibrations species are distributed as: $\Gamma_{vib.} = 17A_1 + 6\,A_2 + 9B_1 + 16B_2$. The A_1 and B_2 vibrations are in-plane modes while A_2 and B_1 represent out-of-plane modes. But if the molecule has C_s symmetry group, the 48 normal vibrations would be distributed as $\Gamma_{vib.} = 33\,A' + 15\,A''$. The A' vibrations are in-plane modes while A'' represents out-of-plane modes. In agreement with C_{2v} point group symmetry, all vibrations are active both in IR and in Raman absorption.

On account of obtaining the spectroscopic features of IPA, a wavenumber calculation analysis has been performed. The theoretical results are in good accordance with the experimental ones especially by using B3LYP method. The calculated and tentative wavenumbers are given in Table 7. The experimental and theoretical infrared and Raman spectra of IPA are shown in Fig. 11. It should be noted that the calculations are performed for the isolated molecule in vacuum, while experiments are recorded for solid samples; therefore, there are some small disagreements between theory and experiment naturally.

4.5.1. C—H vibrations

The aromatic and hetero-aromatic structures demonstrate the subsistence of the C—H stretching vibrations in the 2900–3100 cm^{-1} range [47,48]. This important band is typically exhibited as a

Table 5
Analysis of molecular surface based on blue and red point numbers (Fig. 10).

Point no	Minimum			Maximum		
	a.u.	eV	kcal/mol	a.u.	eV	kcal/mol
1	−0.00346	−0.09424	−2.17302	0.020630	0.561383	12.94477
2	−0.01761	−0.47912	−11.0478	0.001688	0.045936	1.059223
3	−0.01765	−0.48030	−11.0751	0.020591	0.560303	12.91989
4	−0.04830	−1.31441	−30.3087	0.082479	2.244358	51.75205
5	−0.04831	−1.31448	−30.3102	0.017615	0.479332	11.05279
6	−0.01764	−0.48004	−11.0692	0.03472	0.944785	21.78555
7	−0.01764	−0.48005	−11.0693	0.082536	2.245921	51.78808
8	−0.00347	−0.09430	−2.17442	0.020615	0.560966	12.93516
9				0.001708	0.046469	1.071516
10				0.020550	0.559200	12.89445

Table 6
Experimental and theoretical, ^{1}H and ^{13}C NMR isotropic chemical shifts (with respect to TMS) of IPA by DFT (B3LYP/6-311++G(d,p) method.

Atoms	Exp.	Monomer	Dimer	Atoms	Exp.	Monomer	Dimer
C(1)	133.96	134.82	133.84	H(13)	8.46	9.16	9.96
C(2)	130.55	138.53	137.60	H(14)	8.11	8.23	9.38
C(3)	133.96	134.82	132.67	H(16)	8.11	8.23	9.56
C(4), C(6)	131.84	138.94	142.65	H(15)	7.55	7.75	8.57
C(5)	129.58	134.65	133.94	H(17)	–	6.67	7.29
C(7)	167.25	177.59	171.27	H(18)	13.10	6.67	13.92
C(10)	167.25	177.59	177.41				

multiplicity of weak to moderate bands, compared with the aliphatic C—H stretch [49]; so in this study, we obtained weak broad peaks from FT-IR spectrum at about 3100 cm^{-1} which are assigned to asymmetric C—H stretching vibration of IPA. This is due to the decrease of dipole moment caused by the reduction of negative charge on the carbon atom. This reduction occurs because of the electron withdrawal on the carbon atom by the substituent due to the decrease of inductive effect, which in turn is caused by the increased chain length of the substituent [50].

Aromatic C—H stretching modes, four adjacent hydrogen atoms around the benzene ring, predicted in the range of 3047–3098 as pure modes by B3LYP functional of DFT. These aromatic stretching modes occur between ν3–ν6. As indicated by TED, these modes involve exact contribution of ≥98% suggesting that they are very pure stretching modes. The recorded peaks at 3074, 3091 cm^{-1} in FT-IR and 2939, 3082 cm^{-1} in FT-Raman are assigned to C—H stretching modes of the molecule and these modes are calculated at 3048–3101 cm^{-1} for dimer structure by using the B3LYP/6-311++G(d,p) method.

The C—H in-plane-bending vibrations in aromatic compounds characterized by several medium to strong intensity bands in the region between 1300 and 1000 cm^{-1}. The C—H out-of-plane bending vibrations give rise to intense bands in the region between 1000 and 650 cm^{-1} [51,52]. When there is in-plane interaction above 1200 cm^{-1}, a carbon and its hydrogen usually move in opposite direction [51]. In this case, the C—H in-plane bending vibrations are observed at 1166 cm^{-1} in FT–Raman and 1073, 1097, 1162, and 1278 cm^{-1} in FT-IR spectrum.

Table 7
Comparison of the calculated harmonic frequencies and experimental (FT-IR and FT-Raman) wavenumbers (cm^{-1}) of IPA using by B3LYP method 6-311++G(d,p) basis set.

Modes		Experimental		Monomer		Dimer	
	Sym.[a]	FT-IR	FT-Raman	Unscaled freq.	Scaled freq.	Scaled freq.	TED[b] (10%)
ν1	A_1		3658	3770	3612	3580, 3580	νOHsym (100)
ν2	B_2	3456	3380	3770	3612	3116, 3042	νOHasym (100)
ν3	A_1	3091		3234	3098	3101, 3101	νCH (99)
ν4	A_1	3074	3082	3205	3071	3075, 3075	νCH (98)
ν5	B_2			3201	3066	3070, 3070	νCH (99)
ν6	A_1		2939	3181	3047	3048, 3048	νCH (98)
ν7	A_1	1690		1792	1717	1715, 1715	νC = O (82)
ν8	B_2		1635	1785	1710	1669, 1664	νC = O (84)
ν9	B_2	1610	1612	1640	1612	1617, 1617	νCC (64)ring, δCCH (10)
ν10	A_1	1580		1627	1599	1602, 1602	νCC (61)ring, δCCH (17)
ν11	B_2	1485		1515	1490	1497, 1497	νCC (32)ring, δCCH (51)
ν12	A_1	1418	1435	1455	1430	1436, 1433	νCC (41)ring, δCCCH (30)
ν13	A_1			1380	1357	1446, 1423	δCOH (26), νCC (22), νCC (18)
ν14	B_2			1357	1334	1353, 1352	νCC (50) ring, δCOH (11)
ν15	B_2	1327	1301	1350	1327	1336, 1336	δCOH (26), νCC (18)ring, νCO (11), δCCH (13)
ν16	B_2	1278		1320	1298	1314, 1313	δCCH (71), νCC (15)ring
ν17	A_1			1221	1201	1283, 1279	δCOH (53), νCC (17)
ν18	B_2	1162	1166	1192	1171	1191, 1190	δCCH (72), νCC (18)ring
ν19	B_2			1171	1151	1173, 1172	δCOH (33), δCCH (19), νCO (15), νCC (12)
ν20	A_1	1097		1139	1120	1139, 1138	δCCH (32), νCC (17)ring, νCO(13)
ν21	B_2			1094	1076	1097, 1097	νCO (37), νCC (17)ring, δCCH (20)
ν22	A_1	1073		1089	1070	1076, 1076	νCC (36)ring, νCO (27), δCCH (16)
ν23	A_1	1000	1002	1018	1000	1001, 1001	νCC (42)ring, δCCC (39)
ν24	B_1			1017	999	996, 996	γCH[τCCCH (86)]
ν25	A_2			978	962	961, 961	γCH[τCCCH (91)]
ν26	B_1	944		963	947	955, 954	γCH[τCCCH (89)]
ν27	B_2			878	863	877, 876	νCC (36), νCO (12), νCC (11)ring, δCCC (11)
ν28	B_1	832	833	847	832	836, 835	γCH[τCCCH (56)], τCCCO (16)
ν29	A_2		789	798	784	812, 785	τCCCO (79), τCOOH (26)
ν30	B_1	728	761	748	736	904, 794	τCCCO (34), τCCCH (27), τCOOH (26)
ν31	A_1	689		732	720	747, 737	δCCC(17), νCO (16), δCO_2 (14), νCC (24)
ν32	B_1	671	654	686	674	738, 736	τCCCC (47), τCCCH (29)
ν33	A_1	655		645	634	665, 659	δCOO (23), δCCC (22), δCCO (14)
ν34	B_2			645	634	635, 635	δCOO(40), δCCO (17), νCO (11)
ν35	A_2	570		589	579	589, 589	γOH[τCCOH (47), τCOOH (40)]
ν36	B_1			567	557	677, 677	γOH[τCCOH (58), τCOOH (25)]
ν37	B_2	536	501	544	534	558, 542	δCCC (44), δCCO (41)
ν38	A_1	453		470	462	486, 471	δCCO (69)
ν39	A_2	438	424	441	434	454, 452	τCCCO (28), τCCCC (22), τCCOH (13), τCCCH (10)
ν40	B_1	412		422	415	423, 422	τCCCC (55), τCCCH (17)
ν41	B_2		382	390	383	411, 386	δCCC (40), νCC (25)ring, δCOO (13)
ν42	A_1			348	342	362, 353	νCC (49), δCCC (15), δCOO (11), δCCO (10)
ν43	B_2		205	253	249	287, 161	δCCC (53), δCCO (44)
ν44	A_2			179	176	191, 185	τCCCC (50), τCCCH (24), τCCCO (13)
ν45	B_1			142	140	155, 150	τCCCC (43), τCCCO (27)
ν46	A_1		118	135	132	269, 176	δCCC (74), δCCO (16)
ν47	B_1		79	56	55	87, 53	τCCCO (83)
ν48	A_2		43	51	50	59, 46	τCCCO (96)

[a]Sym.: symmetry, [b]TED: total energy distribution, ν; stretching, δ; in plane bending, τ; torsion, γ; out of plane bending, *sym*; symmetric, *asym*; asymmetric.

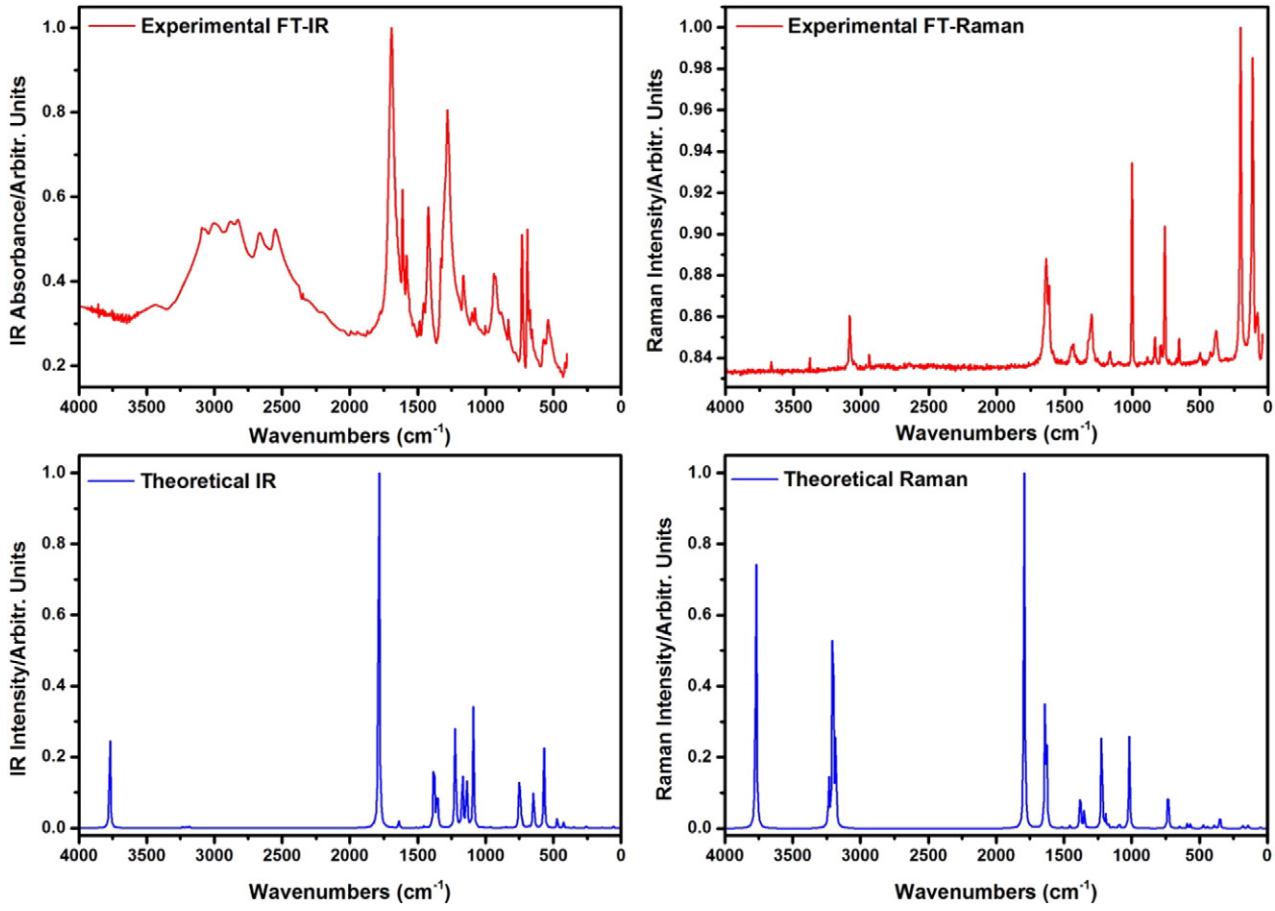

Fig. 11. The experimental and calculated infrared and Raman spectra of IPA.

The same vibrations are calculated between 1070 and 1298 cm^{-1} by B3LYP method. The C—H in-plane bending vibrations have substantial overlapping with the ring C—C stretching vibrations. The absorption bands arising from C—H out-of-plane bending vibrations are usually observed in the region at 675–1000 cm^{-1} [53,54]. The bands are usually very weak in intensity in this region. The FT-IR bands at 944 and 832 cm^{-1} and FT-Raman band at 833 cm^{-1} are assigned to C—H out-of-plane bending vibration. The calculated values of C—H out-of-plane bending vibration also fall in the region of 832–999 cm^{-1} by B3LYP/6-311++G(d,p) method. Both the in-plane and out-of-plane bending vibrations are described as mixed modes.

4.5.2. CO, C—O and O—H, stretching vibrations

Due to the CO stretching vibration, carboxylic group is usually observed a single band in the 1800–1700 cm^{-1} [55–57]. Atac et al. [55] assigned C—O stretching vibration at 1622 cm^{-1} in IR and calculated at 1714 cm^{-1}. In solid state, most of the carboxylic acids exist in dimeric form because of the inter-molecular hydrogen bonding between two —COOH groups. In such a case, two ν(C = O) vibrations are expected: one that is Raman active (symmetric stretching vibration) and the other one (anti-symmetric stretching vibration) is IR active only. Therefore, the CO stretching mode ν7 and ν8 is observed at 1690 cm^{-1} in FT-IR spectrum and 1635 cm^{-1} in FT-Raman spectrum. The theoretical value of CO band is computed at 1717 and 1710 cm^{-1}, respectively. However, the CO stretching mode of dimer conformation was calculated 1664, 1669, 1715, and 1715 cm^{-1} which is in very good agreement with experimental data when the hydrogen-bonding effect is taking into consideration. Two other characteristic carboxylic group vibrations are: C—O stretching ν(C—O) and C—O—H in-plane bending ν(C—OH) which are expected in the 1100–1450 cm^{-1} region depending on whether monomeric, dimeric, or other hydrogen bonded species are present [53,58,59]. The bands observed in FT-IR spectrum at 1073 and 1327 cm^{-1} assigned as C—O stretching and C—OH in-plane bending vibrations. These peaks are calculated as combination of several modes at 1070, 1076, 1151, 1201, 1327 and 1357 cm^{-1}, which exactly coincide with experimental values respectively.

The isolated hydroxyl group absorbs strongly in the region 3700–3400 cm^{-1} [56,57,60]. This may be combined effect of intermolecular hydrogen bonding. Koczoń et al. [61] assigned OH stretching vibration at 3447 cm^{-1} IR and calculated at 3651 cm^{-1}. In this study, this band is recorded at 3380 and 3658 cm^{-1} (FT-Raman) and 3456 cm^{-1} (FT-IR), and predicted to be located at 3612 cm^{-1}. This mode is a pure stretching mode as expected and evidenced from TED calculations with almost 100% contribution. The carboxylic acid dimer is formed by strong hydrogen bonding in the solid and liquid phase. This study showed that there was a frequency downshift of O—H stretching vibration in dimer due to the presence of intermolecular interaction. One can see O—H stretching vibration calculated at 3580, 3116 and 3042 cm^{-1} for dimeric structure, which was in agreement with the interpretation above. The OH in-plane bending occurs between 1440 and 1395 cm^{-1} and out-of-plane bending occurs between 960 and 875 cm^{-1} [62,63]. The O—H out of plane bending vibrations were observed at 570 and 728 cm^{-1} in FT-IR, at 789 and 761 cm^{-1} in FT-Raman. We calculated the out-of-plane bending vibrations (ν29, ν30, ν35 ν36) at 784, 736, 579, and 557 cm^{-1}. The O—H in-plane bending modes and out-of-plane bending vibration values in dimer conformation are either higher or lower depending on the effect of the hydrogen bonding through the carboxyl groups.

4.5.3. Ring carbon vibrations

The ring aromatic carbon–carbon stretching vibrations occur in the region 1430–1625 cm^{-1}. In general, the bands are of variable intensity and are observed at 1625–1590, 1575–1590, 1470–1540, 1430–1465 and 1280–1380 cm^{-1} from the frequency ranges given by Varsanyi [47] for the five bands in the region. The ring stretching vibrations are very important and highly characteristic of the aromatic ring itself. Generally, the C—C stretching vibrations in aromatic compounds form the strong bands. For aromatic six membered rings, there are two or three bands in this region due to skeletal vibrations, the strongest usually being at about between 1500 and 1600 cm^{-1}. In the case where the ring is conjugated further a band at about 1418 and 1610 cm^{-1} is also observed in FT-IR region. Most of the ring modes are altered by the substitution to aromatic ring. According to the TED column, they are signed the C—C vibrations in (ν9–ν23). All bands are observed in the expected range. Their calculated values are at 1000, 1070, 1076, 1120, 1171, 1201, 1298, 1327, 1334, 1357, 1430, 1490, 1599 and 1612 cm^{-1} by B3LYP/6-311++G(d,p) method and the values show excellent agreement with experimental data. All these vibrations except two appeared with mixed modes in TED.

The ring deformation, torsion and CCC bending modes are mixed with other modes. The calculated wavenumbers of these modes almost coincide with experimental data after scaling. The ring deformation, torsion and out-of-plane CCC bending modes are obtained in a large region like vibrational modes of the studied molecule. Therefore, these modes will not be discussed here. Also the TEDs of these vibrations are not pure modes as it is evident from the last column of Table 7.

4.5.4. Characteristic wavenumbers

IPA molecule is a very classical system to study intermolecular hydrogen bonding effects. The calculated wavenumbers for dimer (intermolecular hydrogen bonding) IPA shown in Fig. 2 are tabulated in Table 7. As seen in table, intermolecular hydrogen bonding effect through the carboxyl groups is clearly observed (ν1, ν2, ν30, ν35, ν36,). These results are in agreement with literatures [64–68].

The correlation graphics between the experimental and calculated wavenumbers for monomer and dimer structures of the title molecule are represented in Fig. S4. The relations between the calculated (monomer and dimer) and experimental wavenumbers (ν_{exp}) are usually linear and described by the following equation:

$$\nu_{cal}(cm^{-1}) = 0.9787\nu_{exp} + 14.371 \left(R^2 = 0.9990\right) \text{ for Infrared}$$

$$\nu_{cal}(cm^{-1}) = 0.9780\nu_{exp} + 6.0236 \left(R^2 = 0.9978\right) \text{ for Raman.}$$

The performances of the B3LYP method with respect to the prediction of the wavenumbers within the molecule are quite close.

4.6. Thermodynamic properties

The zero-point vibrational energy, rotational constants, specific heat capacity, thermal energy, entropy and dipole moment of the most stable structure of IPA by DFT/B3LYP/6-311++G(d,p) method at 298.15 K in the ground state are listed in Table 8 as the value of thermodynamic parameters. The global minimum energy obtained for C_{2v}, C_s and C_1 symmetry −609.5838780, −609.5838791 and −609.5838123 a.u, respectively. The entropy value (98.917 cal mol^{-1} K^{-1}) of C_{2v} symmetry of IPA is smaller than C_s and C_1 symmetry ones (bigger than 100 cal mol^{-1} K^{-1}).

Also using the B3LYP with 6-311++G(d,p) basis set is the standard statically thermodynamic functions: heat capacity (C) entropy (S) and enthalpy changes (H) for the IPA were calculated from the theoretical harmonic frequencies and listed in Table 8 according to vibrational analysis. To achieve thermodynamic functions, the temperature increased from 100 to 700 K, and varied every 50 K due to the fact that the molecular vibrational intensities increase with temperature. All results of thermodynamic results of the title molecule presented in Table 9.

Table 8
The calculated thermodynamical parameters of IPA at 298.15 K for all symmetry of C11 conformer in the ground state at the B3LYP/6-311++G(d,p) level.

Parameters	C_{2v} symmetry	C_s symmetry	C_1 symmetry
SCF energy (a.u.)	−609.5838780	−609.5838791	−609.5838123
Zero point vib. Energy (kcal/mol)	81.53429	81.54038	81.53723
Rotational constants (GHz)	1.82648	1.82684	1.82678
	0.59195	0.59214	0.59213
	0.44706	0.44719	0.44718
Specific heat, Cv (cal mol^{-1} K^{-1})	37.664	37.66	37.663
Entropy, S (cal mol^{-1} K^{-1})	98.917	100.289	100.305
Dipole moment (Debye)	0.9381	0.9429	0.9383
Imaginary frequencies	–	–	–

To see correlation equations the heat capacity, entropy, and enthalpy change parameters were fitted with the increasing temperatures by quadratic formulas and the corresponding fitting factors (R^2) for these thermodynamic properties are 0.9993, 1.000 and 0.9998, respectively. The equations are given the follow area and the correlation graphics were also plotted and given in Fig. 12.

$$C^0_{p,m} = 0.9651 + 0.1438T - 6.6179 \times 10^{-5}T^2 \left(R^2 = 0.9993\right)$$

$$S^0_m = 54.7495 + 0.1612T - 4.4138 \times 10^{-5}T^2 \left(R^2 = 1.0000\right)$$

$$H^0_m = -0.5260 + 0.0115T + 4.633 \times 10^{-5}T^2 \left(R^2 = 0.9998\right).$$

To provide useful info for the further study on the IPA, all the thermodynamic data can be presented. These data can be utilized to calculate the other thermodynamic energies according to relationships of thermodynamic functions and to estimate directions of chemical reactions according to the second law of thermodynamics in thermochemical field. Notice: all thermodynamic calculations were done in gas phase and they could not be used in solution.

4.7. Mulliken atomic charges

The Mulliken atomic charges of IPA molecule and its dimer form are listed in Table 10. Mulliken atomic charges are obtained by using DFT/B3LYP method 6-311++G(d,p) basis set. By virtue of the reactive atomic charges play an important role in the application of quantum mechanical calculations the molecular system. The charge of C atoms attached to COOH groups is showed positive distribution while the others

Table 9
Thermodynamic properties of IPA molecule at different temperatures at the B3LYP/6-311++G(d,p).

T (K)	C (cal mol^{-1} K^{-1})	S (cal mol^{-1} K^{-1})	H (kcal/mol K^{-1})
100	15.691	70.047	1.265
150	20.792	78.157	2.273
200	26.403	85.470	3.552
250	32.187	92.426	5.115
298.15	37.664	98.917	6.894
300	37.870	99.163	6.967
350	43.254	105.716	9.096
400	48.218	112.086	11.484
450	52.708	118.263	14.109
500	56.725	124.238	16.946
550	60.297	130.005	19.972
600	63.471	135.563	23.168
650	66.295	140.916	26.512
700	68.817	146.070	29.991

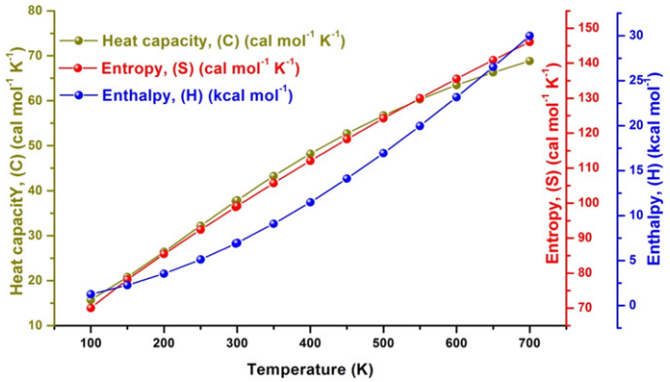

Fig. 12. Correlation graphic of heat capacity, entropy, enthalpy and temperature for IPA.

negative in the aromatic ring. The C_1, C_3, and C_7, C_{10} and O_8, O_{11}, and O_9, O_{12} atoms have the same magnitude due to the symmetry of the title molecule (C_{2v} point group symmetry). Similar state is seen for charges of the hydrogen atoms. The charge of H atoms is positive for all of them both monomer and dimer but they are increasing in the dimer structure of molecule for each other. The hydrogen atoms have a positive charge, which is an acceptor atom in molecules.

4.8. Nonlinear optical properties and dipole moment

To have electronic dipole moment, molecular polarizability, anisotropy of polarizability, and molecular first hyperpolarizability of IPA molecule, the polarization properties were calculated. The polarizability and hyperpolarizability tensors (α_{xx}, α_{xy}, α_{yy}, α_{xz}, α_{yz}, α_{zz} and β_{xxx}, β_{xxy}, β_{xyy}, β_{yyy}, β_{xxz}, β_{xyz}, β_{yyz}, β_{xzz}, β_{yzz}, β_{zzz}) are used a frequency job output file of Gaussian. The units of α and β been converted into electronic units (esu) (α; 1 a.u. $= 0.1482 \times 10^{-24}$ esu, β; 1 a.u. $= 8.6393 \times 10^{-33}$ esu) due to the Gaussian output were in atomic units (a.u.). The equations of the mean polarizability (α), anisotropy of polarizability ($\Delta\alpha$) and the average value of the first hyperpolarizability $\langle\beta\rangle$ are given in the following:

$$\alpha_{tot} = \frac{1}{3}\left(\alpha_{xx} + \alpha_{yy} + \alpha_{zz}\right)$$

$$\Delta\alpha = \frac{1}{\sqrt{2}}\left[\left(\alpha_{xx}-\alpha_{yy}\right)^2 + \left(\alpha_{yy}-\alpha_{zz}\right)^2 + \left(\alpha_{zz}-\alpha_{xx}\right)^2 + 6\alpha_{xz}^2 + 6\alpha_{xy}^2 + 6\alpha_{yz}^2\right]^{\frac{1}{2}}$$

Table 10
Comparison of Mulliken charges of IPA using by B3LYP/6-311++G(d,p) basis set for monomer and dimer of C11 conformer.

Atoms	Monomer	Dimer
C1/19	0.648	0.930
C2/20	−1.150	−0.957
C3/21	0.648	0.549
C4/22	−0.509	−0.587
C5/23	−0.074	−0.475
C6/24	−0.509	−0.504
C7/25	0.234	0.056
O8/26	−0.287	−0.268
O9/27	−0.186	−0.279
C10/28	0.234	0.087
O11/29	−0.287	−0.338
O12/30	−0.186	−0.414
H13/31	0.251	0.327
H14/32	0.190	0.292
H15/33	0.191	0.282
H16/34	0.190	0.259
H17/35	0.301	0.395
H18/36	0.301	0.645

$$\langle\beta\rangle = \left[\left(\beta_{xxx}+\beta_{xyy}+\beta_{xzz}\right)^2 + \left(\beta_{yyy}+\beta_{yzz}+\beta_{yxx}\right)^2 + \left(\beta_{zzz}+\beta_{zxx}+\beta_{zyy}\right)^2\right]^{\frac{1}{2}}.$$

The electronic dipole moment {μ_i (i = x, y, z), total dipole moment $\mu_{tot} = (\mu_x^2 + \mu_y^2 + \mu_z^2)^{\frac{1}{2}}$, and the parameters described above for IPA molecule are given in Table 11.

It is well known that the higher values of dipole moment, molecular polarizability, and hyperpolarizability are important for more active NLO properties. Our title molecule has relatively homogeneous charge distribution and it does not have large dipole moment. The calculated value of dipole moment was found to be 0.9381 Debye. The highest (only) value of dipole moment is observed for component μ_z. In this direction, this value is equal to −0.9381 D, μ_x and μ_y is the smallest one as zero. The polarizability and anisotropy of the polarizability of the title molecule are calculated as 15.8426×10^{-24} esu and 18.6728×10^{-24} esu, respectively. The magnitude of the molecular hyperpolarizability β, is one of the important key factors in a NLO system. The B3LYP/6-311++G(d,p) calculated first hyperpolarizability value (β) of the headline molecule is equal to $1820.6505 \times 10^{-33}$ esu. If we compare the common values of urea; the first hyperpolarizability, polarizability and anisotropy of the polarizability values of IPA are larger than those of urea.

5. Conclusions

The UV–Vis, ^{1}H and ^{13}C NMR, FT-IR and FT-Raman spectral analysis of the title molecule were presented both experimentally and theoretically. Conformational energy and entropy analysis via calculations of DFT/B3LYP/6-311++G(d,p) level of theory show that the most stable conformer defined as C11 conformer with C_{2V} point group symmetry. The calculated and the experimental electronic spectrum recorded using UV–Vis spectrometer in water can be modeled by fitting with antisymmetrized Gaussians successfully. This modeling helps to describe the experimental spectrum quantitatively. To study reactivity given that an approaching electrophile will be attracted to negative regions (where the electron distribution effect is dominant) the MEP also given. ^{13}C and ^{1}H NMR spectra were computed and recorded for the evaluations of the magnetic properties of the title molecule. Chemical shift values are consistent with the symmetry of the molecule; however, due to carboxylic groups, some unexpected values are observed in ^{1}H NMR spectrum of the dimer structure. Dimerization changes the magnetic environment of the carboxyl groups significantly. Weak interaction profile shows the presence of strong hydrogen bonding in dimer structure. Vibrational mode assignments are determined on the basis of TED analysis. All geometrical and vibrational properties agree well between theory and experiments. From top to the bottom, the computed values are compared with experimental and showed acceptable good correlations.

Table 11
The dipole moments μ (D), the polarizability α (a.u.), the average polarizability α_o ($\times 10^{-24}$ esu), the anisotropy of the polarizability Δα ($\times 10^{-24}$ esu), and the first hyperpolarizability β ($\times 10^{-33}$ esu) of IPA.

μ_x	0	β_{xxx}	0.0000
μ_y	0	β_{xxy}	0.0000
μ_z	−0.9381	β_{xyy}	0.0000
μ_0	0.9381	β_{yyy}	0.0000
α_{xx}	8.2564	β_{xxz}	232.5504
α_{xy}	0.0000	β_{xyz}	0.0000
α_{yy}	21.8478	β_{yyz}	−2617.3165
α_{xz}	0.0000	β_{xzz}	0.0000
α_{yz}	0.0000	β_{yzz}	0.0000
α_{zz}	17.4235	β_{zzz}	564.1157
α_{total}	15.8426	β_x	0
Δα	18.6728	β_y	0
		β_z	−1820.6505
		β	1820.6505

Acknowledgments

This work was supported by the Celal Bayar University Research fund through research Grant No.: FBE-2011-70. Some computing resources used in this work were provided by the National Center for High Performance Computing of Turkey (UYBHM) under grant number 400177201 and also part of computation for the work described in this paper was supported by TUBITAK ULAKBIM High Performance Computing Center.

Appendix A. Supplementary data

Supplementary data to this article can be found online at http://dx.doi.org/10.1016/j.saa.2016.03.050.

References

[1] R.J. Sheehan, Ullmann's Encycl. Ind. Chem. Wiley-VCH Verlag GmbH & Co. KGaA, 2000.
[2] J. Gao, Y. Hu, S. Li, Y. Zhang, X. Chen, Spectrochim. Acta A 104 (2013) 41–47.
[3] Y.S. Hwang, J. Liu, J.J. Lenhart, C.M. Hadad, J. Colloid Interface Sci. 307 (2007) 124–134.
[4] C.A. Téllez, E. Hollauer, T. Giannerini, M.I.P. da Silva, M.A. Mondragón, J.R. Rodríguez, V.M. Castaño, Spectrochim. Acta A 60 (2004) 2171–2180.
[5] M. Karabacak, M. Cinar, Z. Unal, M. Kurt, J. Mol. Struct. 982 (2010) 22–27.
[6] Y.Y. Liu, J. Li, J.F. Ma, J.C. Ma, J. Yang, CrystEngComm 14 (2012) 169–177.
[7] S.Y. Yang, L.S. Long, R.B. Huang, L.S. Zheng, S.W. Ng, Inorg. Chim. Acta 358 (2005) 1882–1886.
[8] R. Saxena, L.D. Kandpal, G.N. Mathur, J. Polym. Sci. A 40 (2002) 3959–3966.
[9] L.F. Ma, Q.L. Meng, L.Y. Wang, F.P. Liang, Inorg. Chim. Acta 363 (2010) 4127–4133.
[10] L. Dian-Qing, L. Jiang-Chu, L. Da-Zhuang, W. Fu-An, Fluid Phase Equilib. 200 (2002) 69–74.
[11] B. Han, Z. Li, T. Wandlowski, Anal. Bioanal. Chem. 388 (2007) 121–129.
[12] A. Zafar, J. Yang, S.J. Geib, A.D. Hamilton, Tetrahedron Lett. 37 (1996) 2327–2330.
[13] V.K. Potluri, A.D. Hamilton, J. Supramol. Chem. 2 (2002) 321–326.
[14] A. Shanavas, S. Sathiyaraj, A. Chandramohan, T. Narasimhaswamy, A. Sultan Nasar, J. Mol. Struct. 1038 (2013) 126–133.
[15] W. Nowacki, H. Jaggi, Zeitschrift Für Krist. 109 (1957) 272–283.
[16] J.L. Derissen, Acta Crystallogr., Sect. B: Struct. Crystallogr. Cryst. Chem. 30 (1974) 2764–2765.
[17] R. Alcala, S. Martínez-Carrera, Acta Crystallogr., Sect. B: Struct. Crystallogr. Cryst. Chem. 28 (1972) 1671–1677.
[18] P. Hohenberg, W. Kohn, Phys. Rev. 136 (1964) B864–B871.
[19] A.D. Becke, J. Chem. Phys. 98 (1993) 5648–5652.
[20] C. Lee, W. Yang, R.G. Parr, Phys. Rev. B 37 (1988) 785–789.
[21] M.J. Frisch, et al., Gaussian 09, C3 Revision B.01, Gaussian, Inc., Wallingford, CT, 2010.
[22] N. Sundaraganesan, S. Ilakiamani, H. Saleem, P.M. Wojciechowski, D. Michalska, Spectrochim. Acta A 61 (2005) 2995–3001.
[23] M. Karabacak, M. Cinar, M. Kurt, J. Mol. Struct. 968 (2010) 108–114.
[24] M. Petersilka, U.J. Gossmann, E.K.U. Gross, Phys. Rev. Lett. 76 (1996) 1212–1215.
[25] R. Bauernschmitt, R. Ahlrichs, Chem. Phys. Lett. 256 (1996) 454–464.
[26] C. Jamorski, M.E. Casida, D.R. Salahub, J. Chem. Phys. 104 (1996) 5134–5147.
[27] R. Ditchfield, J. Chem. Phys. 56 (1972) 5688–5691.
[28] K. Wolinski, J.F. Hinton, P. Pulay, J. Am. Chem. Soc. 112 (1990) 8251–8260.
[29] SQM Version 1.0, Scaled Quantum Mechanical Force Field, Green Acres Road, Fayetteville, Arkansas 72703, 2013.
[30] J. Baker, A.A. Jarzecki, P. Pulay, J. Phys. Chem. A 102 (1998) 1412–1424.
[31] N.M. O'Boyle, A.L. Tenderholt, K.M. Langner, J. Comput. Chem. 29 (2008) 839–845.
[32] T. Lu, F. Chen, J. Comput. Chem. 33 (2012) 580–592.
[33] E. Runge, E. Gross, Phys. Rev. Lett. 52 (1984) 997–1000.
[34] W. Humphrey, A. Dalke, K. Schulten, J. Mol. Graph. 14 (1996) 33–38 27–8.
[35] S.K. Lin, J. Chem. Inf. Comput. Sci. 36 (1996) 367–376.
[36] J. Vipin Prasad, S.B. Rai, S.N. Thakur, Chem. Phys. Lett. 164 (1989) 629–634.
[37] M.K. Ahmed, B.R. Henry, J. Phys. Chem. 90 (1986) 1737–1739.
[38] E.R. Johnson, S. Keinan, P. Mori-Sánchez, J. Contreras-García, A.J. Cohen, W. Yang, J. Am. Chem. Soc. 132 (2010) 6498–6506.
[39] E. Runge, E.K.U. Gross, Phys. Rev. Lett. 52 (1984) 997–1000.
[40] M. Chen, U.V. Waghmare, C.M. Friend, E. Kaxiras, J. Chem. Phys. 109 (1998) 6854.
[41] J.R. Rajian, B.R. Hyun, E.L. Quitevis, J. Phys. Chem. A 108 (2004) 10107–10115.
[42] M. Neelakandan, D. Pant, E.L. Quitevis, J. Phys. Chem. A 101 (1997) 2936–2945.
[43] K. Fukui, Science 218 (1982) 747–754.
[44] H.O. Kalinowski, S. Berger, S. Braun, Carbon-13 NMR Spectroscopy, 1988.
[45] S. Sudha, N. Sundaraganesan, M. Kurt, M. Cinar, M. Karabacak, J. Mol. Struct. 985 (2011) 148–156.
[46] A. Coruh, F. Yilmaz, B. Sengez, M. Kurt, M. Cinar, M. Karabacak, Struct. Chem. 22 (2011) 45–56.
[47] G. Varsányi, Assignments for Vibrational Spectra of Seven Hundred Benzene Derivatives, Halsted Press, 1974.
[48] M. Govindarajan, K. Ganasan, S. Periandy, M. Karabacak, S. Mohan, Spectrochim. Acta A 77 (2010) 1005–1013.
[49] J. Coates, in: J. Coates (Ed.), R.A.M. 2000, pp. 10815–10837.
[50] H. Spedding, D.H. Whiffen, Proc. R. Soc. London. Ser. A. Math. Phys. Sci. 238 (1956) 245–255.
[51] H. Sato, J. Dybal, R. Murakami, I. Noda, Y. Ozaki, J. Mol. Struct. 744-747 (2005) 35–46.
[52] P.B. Nagabalasubramanian, M. Karabacak, S. Periandy, Spectrochim. Acta A 85 (2012) 43–52.
[53] R.M. Silverstein, G.C. Bassler, T.C. Morrill, Spectrometric Identification of Organic Compounds, Wiley, 1991.
[54] P.B. Nagabalasubramanian, M. Karabacak, S. Periandy, Spectrochim. Acta A 82 (2011) 169–180.
[55] A. Atac, M. Karabacak, C. Karaca, E. Kose, Spectrochim. Acta A 85 (2012) 145–154.
[56] G. Socrates, Infrared and Raman Characteristic Group Frequencies: Tables and Charts, Wiley, 2001.
[57] B. Smith, Infrared Spectral Interpretation: A Systematic Approach, 1998.
[58] D. Lin-Vien, N.B. Colthup, W.G. Fateley, J.G. Grasselli, The Handbook of Infrared and Raman Characteristic Frequencies of Organic Molecules, Academic Press, 1991.
[59] M. Karabacak, Z. Cinar, M. Cinar, Spectrochim. Acta A 79 (2011) 1511–1519.
[60] M. Karabacak, E. Kose, A. Atac, Spectrochim. Acta A 91 (2012) 83–96.
[61] P. Koczoń, J.C. Dobrowolski, W. Lewandowski, P. Mazurek, J. Mol. Struct. 655 (2003) 89–95.
[62] R.M. Silverstein, F.X. Webster, D.J. Kiemle, Spectrometric Identification of Organic Compounds, John Wiley & Sons, 2005.
[63] M. Karabacak, L. Sinha, O. Prasad, Z. Cinar, M. Cinar, Spectrochim. Acta A 93 (2012) 33–46.
[64] M. Karabacak, M. Kurt, J. Mol. Struct. 919 (2009) 215–222.
[65] Y. Akkaya, S. Akyuz, Vib. Spectrosc. 42 (2006) 292–301.
[66] M. Karabacak, M. Kurt, Spectrochim. Acta A 71 (2008) 876–883.
[67] M. Karabacak, M. Cinar, S. Ermec, M. Kurt, J. Raman Spectrosc. 41 (2010) 98–105.
[68] M. Karabacak, E. Kose, M. Kurt, J. Raman Spectrosc. 41 (2010) 1085–1097.